IEEE Access
Multidisciplinary ⋮ Rapid Review ⋮ Open Access Journal

Received 27 November 2022, accepted 15 December 2022, date of publication 21 December 2022,
date of current version 29 December 2022.

Digital Object Identifier 10.1109/ACCESS.2022.3231443

RESEARCH ARTICLE

Robust Tube-Based Model Predictive Control for Autonomous Vehicle Path Tracking

KANGLE HU AND KAI CHENG
School of Mechanical and Aerospace Engineering, Jilin University, Changchun 130022, China
Corresponding author: Kai Cheng (chengkai@jlu.edu.cn)

This work was supported by the National Key Research and Development Program of China under Grant 2016YFC0802703.

ABSTRACT In real-world driving scenarios, the model mismatch can severely impair the robustness of the tracking system controlled by Model Predictive Control (MPC). Tube-based MPC (TMPC) addresses this problem by keeping the model mismatch error in an invariant tube. The TMPC algorithms, however, cannot deal with state-dependent uncertainty since TMPC relies on the fixed tubes. This paper presents a practical algorithm for improving the capability of TMPC to handle multiplicative uncertainty. Firstly, this algorithm adopts a Homothetic Tube-based MPC (HTMPC) framework to optimize the system's future trajectory and tube geometry simultaneously, which dynamically resizes tubes according to uncertainty and the system's current state. Secondly, this algorithm provides both the feasible formulation of the tube and the homothetic factor with low computational complexity. Thirdly, we aim to systematically evaluate the algorithm's robustness by the simulations of different scenarios where the system parameters and the measurement noises might change over time. We have conducted and analyzed the Monte-Carlo simulations to compare the robustness and tracking capability of the proposed algorithm and other control algorithms. The comparative analysis shows that the HTMPC algorithm provides a higher level of performance than MPC and TMPC, and it performs closely to the robust controller based on the immersion and invariance (I&I) principle.

INDEX TERMS Autonomous vehicles, immersion and invariance (I&I), path tracking, robustness, state-dependent uncertainty, tube model predictive control.

I. INTRODUCTION

Due to the high non-linearity of the vehicle system and the uncertain disturbances caused by the driving environment, *robustness* is a critical issue in the control design. A robust controller should cope with disturbances and parameter uncertainties such as tire cornering stiffness. Hence, some researchers adopted many robust control methods to maintain robustness and tracking performance. State-of-art control approaches, including Fuzzy Control [1], Optimal Control [2], Sliding Mode Control (SMC) [3], Flatness-based Control (FLAT) [4], Immersion and Invariance Principle (I&I) [5], Robust H_∞ [6], Model Predictive Control (MPC), and Reinforced Learning [7], are developed successfully and likely to be applied to the vehicle control at complex driving. A robust T-S fuzzy output- feedback controller has been developed for the automated driving considering the obstacle avoidance [8]. Sliding mode control are effective for compensating the model parameter variations. However, SMC can output aggressive control action: tracking performance are significantly reduced due to the rapid change of the control input. Flatness-based control has the advantage of high tracking precision and stability. However, FLAT show some weakness in rejecting the noise. Additionally, FLAT is sensitive to the model parameter variation. I&I and optimal control are robust against measurement noise. Robust H_∞ requires extensive computation and behaves conservatively. Most approaches' main disadvantage is not explicitly considering vehicles' state and actuator constraints. By contrast, MPC has been widely applied to vehicle control because it can systematically utilize system's current sates and satisfy Multiple-Input Multiple-Output (MIMO) constraints. The explicit modeling

The associate editor coordinating the review of this manuscript and approving it for publication was Ton Duc Do.

of autonomous vehicles is inherently subject to uncertainties, for example the variation in tire cornering stiffness. Thus, the reliance on accurate modeling makes MPC susceptible to modeling mismatch errors and external disturbances, leading to poor performance or instability. Therefore, it is difficult to essentially eliminate the environment's interference through the open-loop feedback law of MPC. In recent years, researchers have proposed several robust MPC techniques to strengthen the robustness of MPC under uncertainty [9]. One of these methods is a so-called feedback min-max optimization [10], which provides a robust conservative solution for the optimization problem with bounded disturbances by considering all possible uncertainties realizations. Because of its inherent complexity, this method helps search for a more conservative but efficient approximation of the optimal solution, which is computationally tractable in practice by utilizing the linear matrix inequality (LMI) [11].

Tube-based MPC (TMPC) is an efficient alternative to the min-max MPC, which decomposes the robust MPC into a robust local controller and an online open-loop nominal MPC controller. The nominal MPC drives the nominal system states to equilibrium. At the same time, the robust local control steers the error system into a tiny region (so-called "*tube*") near the trajectory of the nominal system. The tube design utilizes the information of the upper and lower bounds of the disturbance set. The feedback law can ensure that the error system never goes out of the tube under any admissible disturbance. Therefore, the TMPC keeps the actual trajectory of the uncertain system inside the nominal-trajectory-centered region. Researchers in [12] and [16] applied the TMPC approach for vehicle path tracking to deal with external disturbances. In [13], TMPC algorithm presented strong robustness under additive disturbance, such as the wind, road slope, and estimation errors. Furthermore, the variation of tire characteristics directly influences vehicle tracking performance [14]. Tire characteristics are related to the temperature, wear, and road friction coefficient. This paper focuses on applying the TMPC algorithm considering the variation of tire cornering stiffness. Wang et al. [15] proposed an adaptive TMPC to deal with uncertainties, which directly estimates uncertain tire cornering stiffness online by a recursive least square (RLS) estimator. The robustness of the control system highly depends on the accuracy of estimation. Sun et al. [16] proposed a robust tube MPC method based on tube-division for vehicle path tracking control considering the uncertain friction coefficient, which selected a corresponding tube from a sequence of the candidate tubes based on the vehicle states. TMPC approach needs to ensure the robustness by minimizing the tube size. A minimal tube typically leads to a high-bandwidth corrective controller that aggressively behaves to any disturbances, including noise or parameter perturbation. Aggressive behavior can severely degrade performance or exceed the actuator limit for vehicle control systems that rely on onboard sensors for estimation or perception. Therefore, modifying the tube geometry online would be advantageous compared to the fixed tube geometry [17]. It is a crucial focus of this paper how to parameterize the tube to strike a good balance between computational complexity and robustness of the control system.

Because of the conservative property of rigid tubes, researchers have proposed multiple kinds of dynamic tube as an alternative, including homothetic tube [18], [19] and elastic tube [20]. According to [21], homothetic tube consists of a sequence of scaled copies of the basic shape set, represented by the tube centers (i.e., the nominal system trajectory) and the scaling factor. Homothetic TMPC (HTMPC) algorithm treats the state and control tubes as homothetic tubes. Thus, the HTMPC algorithm is of advantage to dynamically adjust tube geometry and the constraints to avoid constraint violation given that the system states are close to the limit. In [22], a much more flexible parameterization has been studied, allowing the online computation of tube shape sets. While the HTMPC has been applied to the constrained linear systems under additive disturbance, the uncertainty enters multiplicatively into the control system in the case of parametric uncertainty. In this way, researchers developed the concept of HTMPC for controlling multiplicative uncertain systems [23]. In [24], Hanema et al. proposed the so-called heterogeneous tube, where the parameterization of the tube cross-sections can vary over the prediction horizon. This parameterization reduces conservatism and provides more flexibility in constructing the tubes. The homothetic tube-based economic MPC synthesis for constrained linear discrete-time systems has integrated a moving horizon estimator to achieve constraint satisfaction [25]. Nevertheless, one of the drawbacks of this algorithm is its computational burden. The researchers in [25] pointed out that the solution is to adopt the polyhedral or ellipsoid sets to approximate the exact robust invariant sets. Thus, it needs more in-depth investigation on obtaining a feasible tube shape set in an easy-to-calculate way.

Current literature on TMPC in vehicle path-tracking usually utilizes a matrix polytope to represent the tube shape set in case of parametric uncertainty [26], [27]. This tube parameterization can accurately approximate the uncertainty set in the form of a convex hull of its vertices. Gao et al. [28] computed the robust positively invariant set by the complex set computations: the Pontryagin difference and the Minkowski sum. However, the number of vertices can be vast to model high-dimensional uncertainty sets. Thus, if the matrix uncertainty set is structured but not low dimensional, the ellipsoidal modeling approach has advantages in terms of computational complexity and the minimum approximation size [29], [30]. Researchers computed an ellipsoidal invariant set [31] or an ellipsoidal reachability set [32] by means of LMI. Xu et al. [33] proposed the robust positively invariant (RPI) set and the terminal constraint set for the RMPC algorithm in the form of the ellipsoidal set by resolving the LMIs, which realized the accurate tracking control in the presence of the tire cornering stiffness uncertainty. Furthermore, using tubes with ellipsoidal cross-sections allows online minimizing a quadratic cost [34], which enables the shape size of the

tube cross-section to be optimized online by semi-definite programming (SDP) [35]. Thus, this paper establishes an efficient process to obtain the ellipsoidal tube shape set to approximate the exact mRPI set [36]. The optimal size of the tube is determined online by calculating the homothetic factors. Homothetic factors are defined as the decision variable of the HTMPC optimization problem. The solution to the online optimization problem provides an online homothetic factor.

This paper proposes a control framework for the practical application of vehicle systems based on the developed theory of Homothetic TMPC synthesis [19]. The contribution of this paper is the efficient formulation of the dynamics model such that the resulting optimization problem is feasible in real time. This paper will investigate the possible robust performance gains from applying this control framework. Simulink and Carsim simulate a path tracking environment under uncertainties, which validates the robust performance of the controller. Moreover, the existing application of TMPC theory in the vehicle's path tracking has yet to be compared to other robust control methods concerning the robustness to attenuate the uncertainties such as varying tire cornering stiffness. Thus, we systematically compare the proposed method with three control approaches for the vehicle tracking a double lane change path in several specific scenarios to test the robustness in [5], [14], and [15]. The work of this paper therefore can be divided into three parts, including the vehicle modeling, the formulation of the HTMPC control framework, and the co-simulation of different scenarios, illustrated in Fig. 1. The main work of this paper is summarized in the following aspects:

1) We propose a calculation process for a homothetic tube utilizing linear matrix inequality with minimum computational complexity, which can resize the tube geometry in response to the state-dependent uncertainty.
2) This paper presents an HTMPC control framework for a linear path-tracking system where the tube geometry and open-loop nominal trajectory are optimized simultaneously, giving the controller more freedom to adjust the tube to improve its robustness.
3) This paper utilizes a benchmark to evaluate the robustness of control algorithms and quantify their performance in several scenarios involving sensor noise and parametric uncertainties [37].

The rest of this paper is organized as follow. In Section II, the vehicle lateral dynamics, and the vehicle kinematics for path tracking are integrated into a simplified uncertain model. In Section III, we formulate the HTMPC framework. In Section IV, the different simulation results are provided, and the robustness of the proposed strategy is discussed. Finally, the paper ends in Section V with concluding remarks of the work.

II. SYSTEM MODELING

In this research, the vehicle path-following model consists of the vehicle lateral dynamics model and the vehicle tracking-error model. We adopt a 2-Dof bicycle model to describe the lateral dynamics of the vehicle, which has been widely used in automated driving. Furthermore, we have used the modeling technique of approximating the tire dynamics in linear regions to obtain a simplified tire model [11], [38]. The assumptions regarding vehicle modeling and vehicle path following are listed as follows:

1) This study assumes that the vehicle operates at a constant speed of 60 km/h. We assume the longitudinal force of the tire is equal to the road friction and wind resistance. Therefore, this work focus on the tire's side slip and neglects the tire's longitudinal slip.
2) Vehicle motions such as vertical, roll, and pitch are not considered. The normal load of each tire is assumed to remain constant and has no impact on the lateral force of tires. Therefore, the roll stability will not be considered in this work.
3) Tire side-slip angles are expected to be small in normal driving conditions. The tire's side-slip angle β_i is equal to or below the side-slip angle β_i^m that corresponds to the peak force. In consequence, the lateral force of the tire is approximately proportional to the side-slip angle.
4) This work assumes that the relative orientation angle between the vehicle and the desired path is slight, so a linear vehicle model regarding the tracking errors can describe the path tracking.

A. VEHICLE LATERAL DYNAMICS MODEL

The dynamic model of the vehicle is built in two stages. A simplified two-degree of freedom (DOF) 'bicycle' model is proposed in the first step, as shown in Fig. 2. The lateral dynamics of vehicle includes the main features of vehicle motion in normal driving. In the second step, we utilize a linearized tire model that accounts for the uncertainty of tire cornering stiffness. Under the assumption of a constant longitudinal velocity v_x, the lateral dynamics of a vehicle can be expressed as follows:

$$\begin{aligned} m(\dot{v_y} + v_x\omega) &= F_{yf} + F_{yr} \\ I_z\dot{\omega} &= l_f F_{yf} - l_r F_{yr} \end{aligned} \tag{1}$$

For the sake of simplicity of vehicle modeling, the approximate tire model could be substituted for the nonlinear tire model when the tire operates in the linear operating zone. In this case, we utilize the linear function to approximate the relationship between lateral force and side-slip angle:

$$\begin{aligned} F_{yf} &\approx -C_{f0}\beta_f \\ F_{yr} &\approx -C_{r0}\beta_r \end{aligned} \tag{2}$$

where C_{f0} and C_{r0} denote the nominal cornering stiffness of front and rear tires. β_f and β_r denote the side-slip angle of the front and rear tires, respectively, which are determined by linearized vehicle kinematics as:

$$\begin{aligned} \beta_f &= (v_y + l_f\dot{\omega})/v_x - \delta_f \\ \beta_r &= (v_y - l_r\dot{\omega})/v_x \end{aligned} \tag{3}$$

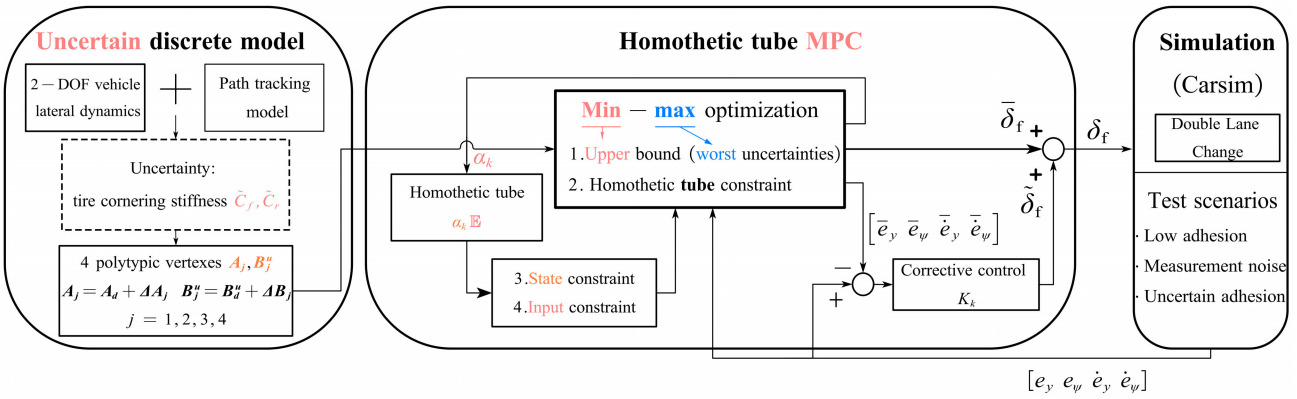

FIGURE 1. General architecture of this paper including three parts: modeling, control framework, and simulation test.

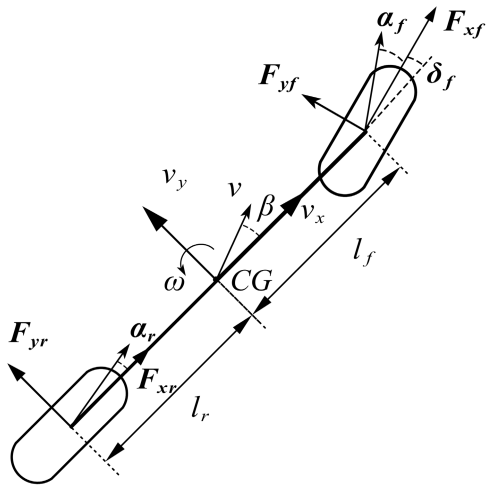

FIGURE 2. Lateral dynamics of autonomous vehicle.

B. UNCERTAIN TIRE MODEL

The proposed vehicle model simplifies tire lateral dynamics as a linear model. However, this simplification will result in a significant mismatch between real and nominal vehicle models. Thus, non-linearity in tire dynamics should be taken into account by the vehicle model. The Fiala brush model may be appropriate for modeling the nonlinear relationship between tire side-slip angle and lateral force as follows:

$$F_{yi} = \begin{cases} a_i \tan\beta_i + b_i |\tan\beta_i| \tan\beta_i + c_i \tan^3\beta_i & \text{if} |\beta_i| \le \beta_i^{sat} \\ -\mu_i F_z \text{sgn}(\beta_i) & \text{otherwise.} \end{cases} \quad (4)$$

where μ_i denotes the friction coefficient. F_z denotes the normal load and the subscript "i" denotes the term f and r corresponding to the front axle and rear axle, respectively. Then, $a_i = -C_{i0}$, $b_i = \frac{C_i^2}{3\mu_i F_z}$, $c_i = -\frac{C_i^3}{27\mu_i^2 F_z^2}$, $\beta_i^{sat} = \tan^{-1}\frac{3\mu_i F_z}{C_i}$. The peak of tire lateral force F_{yi}^{peak} and its corresponding side-slip angle β_i^{peak} can be derived as follows:

$$\begin{aligned} F_{yi}^{peak} &= \mu_i F_{zi} \\ \beta_i^{peak} &= \tan^{-1}\frac{3\mu_i F_{zi}}{C_i} \end{aligned} \quad (5)$$

Additionally, the instantaneous slope of the peak of the tire force concerning the side-slip angle determines the minimum cornering stiffness $C_i^{\min}$: $C_i^{\min} = F_{yi}^{peak}/\beta_i^{peak}$. Tire cornering stiffness varies between the maximum and minimum values in the approximate linear domain. The maximum cornering stiffness, $C_f^{\max}$ and $C_r^{\max}$, are equivalent to the cornering stiffness when the corresponding side-slip angle is zero. We rewrite Eq. (2) to take this characteristic into account:

$$\begin{aligned} &\forall|\beta_i| \le \beta_i^{peak} \ \ \exists|\gamma_i| \le 1: \\ &F_{yf} = -(C_{f0} + \gamma_f \tilde{C}_f)\beta_f \\ &F_{yr} = -(C_{r0} + \gamma_r \tilde{C}_r)\beta_r \\ &\tilde{C}_f = \frac{C_f^{\max} - C_f^{\min}}{2}, \tilde{C}_r = \frac{C_r^{\max} - C_r^{\min}}{2} \\ &C_{f0} = \frac{C_f^{\max} + C_f^{\min}}{2}, C_{r0} = \frac{C_r^{\max} + C_r^{\min}}{2} \end{aligned} \quad (6)$$

where C_{f0} and C_{r0} denote the nominal cornering stiffness that are assumed to be the mean value of maximum and minimum cornering stiffness. $\tilde{C}_f$ and $\tilde{C}_r$ denote the expected range of varying cornering stiffness. With the factor γ_f and γ_r, we describe the degree of cornering stiffness variation influenced by the road adhesion or vertical force of the tire. γ_f and γ_r are uncertain variables that are norm-bound such that $|\gamma_f| \le 1$ and $|\gamma_r| \le 1$.

Remark 1: From the relations in Eq. (6), the lateral force F_{yi} is significantly affected by the term $\gamma_i \tilde{C}_i$. The uncertain cornering stiffness could significantly affect the vehicle's dynamics. A low friction coefficient could reduce the tire lateral force in snow-ice tracks. Thus, it is apparent that the uncertain parameters γ_f and γ_r are closely related to the road adhesion coefficient μ_i. A vehicle's path-tracking strategy needs to minimize the impact of uncertain road friction. We construct a vehicle path tracking model that takes tire uncertainty into account in the next section. The formulation of this model is a state-space model, where the uncertain cornering stiffness affects both the state matrix and input matrix. To address the uncertainty, we propose a homothetic tube-based MPC control framework based on the established works [19].

TABLE 1. Nomenclature.

Symbol	Definition	Unit
m	Vehicle mass	kg
f, r	subscripts denoting front and rear	
I_z	vehicle yaw moment of inertia	kg.m^2
F_{xi}	Longitudinal tire force ($i = f, r$)	N
F_{yi}	Lateral tire force ($i = f, r$)	N
β_f/β_r	Front/rear tire sideslip angle	rad
C_i	Cornering stiffness ($i = f, r$)	(kN/rad)
C_{i0}	Nominal cornering stiffness ($i = f, r$)	(kN/rad)
l_f/l_r	Distance of CG from front/rear axle	m
v_x	Vehicle longitudinal velocity	m/s
v_y	Vehicle lateral velocity	m/s
ω	Vehicle yaw rate	rad/s
ψ	Orientation angle of vehicle body	rad
ψ_d	Desired orientation angle of vehicle body	rad
δ_f	Front wheel steering angle	rad
c_R	Path curvature	1/m
e_ψ	Heading error of vehicle w.r.t. road reference	rad
e_y	Lateral offset of vehicle w.r.t. road reference	m

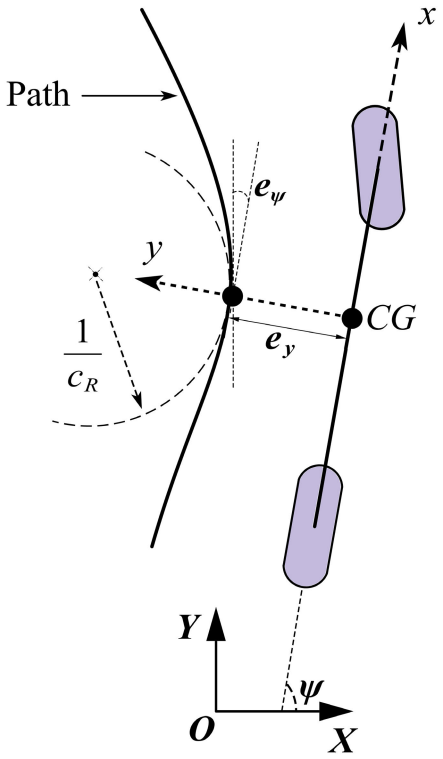

FIGURE 3. Kinematic error-based tracking model of autonomous vehicle.

C. FORMULATION OF PATH TRACKING

We adopt the widely used path following model illustrated in Fig. 3, which illustrates two points representing the actual location of the vehicle's center of gravity (CG) and the target destination on the path. The lateral offset from the CG to the destination point is denoted by e_y. The heading angle error e_ψ is the difference between the orientation angle of the vehicle ψ and the reference orientation angle ψ_d, expressed as $e_\psi = \psi - \psi_d$. Based on a constant longitudinal velocity v_x and a predicted curvature c_R, we obtain the derivative of the desired orientation angle $\dot{\psi}_d = v_x c_R$. The lateral tracking error e_y and yaw angle error e_ψ, and the corresponding derivatives are expressed as follows:

$$\begin{aligned} \dot{e}_y &= v_y + v_x e_\psi \\ \dot{e}_\psi &= \dot{\psi} - \dot{\psi}_d \\ \ddot{e}_\psi &= \ddot{\psi} - \ddot{\psi}_d \\ \ddot{e}_y &= \dot{v}_y + v_x \dot{e}_y \end{aligned} \tag{7}$$

By integrating the vehicle lateral dynamics into the path tracking modeling approach, we eliminate the terms $\dot{v}_y$, $\ddot{\psi}$. Substituting Eq.(1) for Eq.(7), we replace $\ddot{e}_y$ and $\ddot{\psi}$ with e_y, e_ψ and its derivatives $\dot{e}_y$ and $\dot{e}_\psi$, which is expressed as follows:

$$\begin{aligned} \ddot{e}_y = &\frac{C_f}{m}\delta_f - \frac{C_f + C_r}{m v_x}(\dot{e}_y - v_x e_\psi) \\ &+ [\frac{(C_r l_r - C_f l_f)}{m v_x} + v_x](\dot{e}_\varphi + \dot{\varphi}_d) + v_x \dot{e}_\psi \end{aligned} \tag{8}$$

$$\begin{aligned} \ddot{e}_\varphi = &\frac{C_f l_f}{I_z}\delta_f - \frac{C_f l_f - C_r l_r}{m v_x}(\dot{e}_y - v_x e_\psi) \\ &- \frac{(C_r l_r^2 + C_f l_f^2)}{I_z v_x}(\dot{e}_\varphi + \dot{\psi}_d) - \ddot{\psi}_d \end{aligned} \tag{9}$$

By rearranging the relation in Eq. (8-9) into the form of matrix, we can obtain the state-space model as follows:

$$\dot{\mathbf{z}}(t) = (\mathbf{A} + \Delta\mathbf{A_j})\mathbf{z}(t) + (\mathbf{B^u} + \Delta\mathbf{B}_j)\mathbf{u}(t) + \mathbf{B^r}\,\mathbf{w}(t) \tag{10}$$

where $\mathbf{z}(t) = [e_y(t), e_\psi(t), \dot{e}_y(t), \dot{e}_\psi(t)]^T$ is the state vector. $\mathbf{u}(t)$ denotes the control input. $\mathbf{w}(t)$ denotes the path curvature $c_R(t)$. $\mathbf{A}$ and $\mathbf{B}$ denote the nominal matrices of state and input. $\Delta\mathbf{A_j}$ and $\Delta\mathbf{B_j}$ denote the uncertain matrices, which supplement the nominal matrix $\mathbf{A}$ and $\mathbf{B^u}$ to take the uncertainty into account.

Remark 2: Eq. (6) shows that γ_f and γ_r denote the changing degree of the tire cornering stiffness. To formalize the uncertain parameter γ_f and γ_r, we propose a polytope Δ that contains $j = 4$ vertices, Δ_j, equivalent to the minimum and maximum of γ_f and γ_r. γ_f and γ_r are bounded within a range of $[-1, 1]$. Thus, the vertices of the polytope Δ_j can be expressed as follows:

$$\Delta_1 = \begin{bmatrix} 1 & 0 \\ 0 & 1 \end{bmatrix} \Delta_2 = \begin{bmatrix} 1 & 0 \\ 0 & -1 \end{bmatrix}$$
$$\Delta_3 = \begin{bmatrix} -1 & 0 \\ 0 & 1 \end{bmatrix} \Delta_4 = \begin{bmatrix} -1 & 0 \\ 0 & -1 \end{bmatrix}$$

For the simplicity of mathematical formulation, we use the matrix decomposition to deal with the uncertain matrices $\Delta\mathbf{A_j}$ and $\Delta\mathbf{B_j}$, which are expressed as the product of the matrices $\mathbf{B^w}$, $\mathbf{C_y}$, $\mathbf{D_y^u}$ and the vertices Δ_j. The nominal matrices $\mathbf{A}$,$\mathbf{B^u}$,and $\mathbf{B^r}$ and the uncertain matrix $\Delta\mathbf{A_j}$, $\Delta\mathbf{B_j^u}$, are given by:

$$\mathbf{A} = \begin{bmatrix} 0 & 0 & 1 & 0 \\ 0 & 0 & 0 & 1 \\ 0 & -\frac{(C_{f0}+C_{r0})}{m v_x} & \frac{(C_{f0}+C_{r0})}{m} & \frac{(C_{r0}l_r - C_{f0}l_f)}{m v_x} \\ 0 & \frac{(C_{r0}l_r - C_{f0}l_f)}{I_z v_x} & \frac{(C_{r0}l_r - C_{f0}l_f)}{I_z} & -\frac{(C_{r0}l_r^2 + C_{f0}l_f^2)}{I_z v_x} \end{bmatrix}$$

$$\mathbf{B^u} = \begin{bmatrix} 0 \\ 0 \\ \frac{C_{f0}}{m} \\ \frac{C_{f0}l_f}{I_z} \end{bmatrix} \quad \mathbf{B}^r = \begin{bmatrix} 0 \\ 0 \\ \frac{(C_{r0}l_r - C_{f0}l_f)}{m} - v_x^2 \\ -\frac{(C_{r0}l_r^2 + C_{f0}l_f^2)}{I_z} \end{bmatrix}$$
$$\Delta\mathbf{A_j} = \mathbf{B^w}\Delta_j\mathbf{C_y},\ \Delta\mathbf{B_j} = \mathbf{B^w}\Delta_j\mathbf{D_y^u}$$
$$\mathbf{B^w} = \begin{bmatrix} 0 & 0 & -\frac{1}{mv_x} & -\frac{1}{mv_x} \\ 0 & 0 & -\frac{l_f}{I_z v_x} & -\frac{l_r}{I_z v_x} \end{bmatrix}^T$$
$$\mathbf{C_y} = \begin{bmatrix} 0 & 0 & \tilde{C}_f & l_f\tilde{C}_f \\ 0 & 0 & -\tilde{C}_r & l_r\tilde{C}_r \end{bmatrix}$$
$$\mathbf{D_y^u} = \begin{bmatrix} -\tilde{C}_f \\ 0 \end{bmatrix}$$
$$\Delta_\mathbf{j} = \begin{bmatrix} \gamma_f & 0 \\ 0 & \gamma_r \end{bmatrix} \tag{11}$$

Model predictive control algorithm is usually applied to the linear discrete time system. Therefore, we transform the continuous-time model in Eq. (10) into a discrete-time model, expressed as follows:

$$z_{k+1} = (\mathbf{A_d} + \Delta\mathbf{A_j})z_k + (\mathbf{B_d^u} + \Delta\mathbf{B_j})u_k \tag{12}$$

where $\mathbf{A_d}$ and $\mathbf{B_d^u}$ denote the constant matrices discretized from $\mathbf{A}$ and $\mathbf{B^u}$. $\Delta\mathbf{A_j}$, $\Delta\mathbf{B_j}$ denote the uncertain matrices discretized from $\Delta\mathbf{A}$ and $\Delta\mathbf{B}$.

III. HOMOTHETIC TUBE-BASED MPC PATH FOLLOWING CONTROL STRATEGY

Based on the established uncertain path tracking model with four vertices, the control framework can describe the extreme parametric uncertainties due to the changing tire cornering stiffness. In the next step, we propose the min-max optimization problem. The structure of this optimization problem has been illustrated in Fig. 1. The optimization problem can be solved to determine the control action sequence corresponding to the minimized upper bound of the cost function when the control system is assumed to be under the worst-case uncertainty. The actual control input to the vehicle in simulation platform Carsim, namely the steering angle of front axle δ_f, is the summation of the nominal control action $\bar{\delta}_f$ and corrective control action $\tilde{\delta}_f$. The corrective action $\tilde{\delta}_f$ is derived from the corrective control law: $\tilde{\delta}_f = K_k(\hat{z}_k - \bar{z}_k)$, where $(\hat{z}_k - \bar{z}_k)$ denotes the difference between the actual system and nominal state.

A. PROBLEM DEFINITION

The discrete time system used in the control framework is described by $z^+ = \boldsymbol{A}\mathbf{z} + \boldsymbol{B}\mathbf{u} + \mathbf{w}$. $\mathbf{z}$ is the state vector. $\mathbf{u}$ is the control vector. $\mathbf{z}^+$ is the succeeding state vector. $\mathbf{w}$ is the disturbance vector and its values are assumed in the set $\mathbb{W}$, and the matrix pair $(\boldsymbol{A}, \boldsymbol{B}) \in \mathbb{R}^{n\times n} \times \mathbb{R}^{n\times m}$ is unknown due to the parametric uncertainty, but it is assumed to satisfy:$(\boldsymbol{A}, \boldsymbol{B}) \in \mathbb{C}$ with $\mathbb{C} := \text{convh}(\boldsymbol{A_j}, \boldsymbol{B_j})$. The vertices of matrix pair $(\boldsymbol{A_j}, \boldsymbol{B_j})$ are the summation of the nominal matrix $\boldsymbol{A}, \boldsymbol{B^u}$ and the uncertain matrices vertices $\Delta\mathbf{A_j}$, $\Delta\mathbf{B_j}$ in Eq.(11). At any time instant $k \in \mathbb{N}$, the state vector $\mathbf{z_k}$ and the control input u_k are assumed known while the matrix pair $(\boldsymbol{A_k}, \boldsymbol{B_k})$ are not known and may be any arbitrary values $(\boldsymbol{A_k}, \boldsymbol{B_k}) \in \mathbb{C}, i \in \mathbb{N}_{\geq 0}$.

Remark 3: Unpredictable uncertainties could affect the predicted system's state and control action progress due to the uncertain matrices $(\boldsymbol{A_j}, \boldsymbol{B_j})$. Consequently, it is critical to restrict all possible predicted state and their corresponding control input into a feasible bound. The HTMPC framework can achieve this restriction by using the homothetic states and control tubes to describe all possible states and control input. The detailed description of control theory regarding HTMPC can be referred from the established publications [18], [19]. A brief introduction to the theoretical background of HTMPC is presented as follows.

Definition 1: For any non-empty sets $\mathcal{S} \subseteq \mathbb{R}^n, \mathcal{R} \subseteq \mathbb{R}^m$, any control function $\nu(\cdot) : \mathbb{R}^n \to \mathbb{R}^m$, and any $N \in \mathbb{N}_{\geq 1}$, the homothetic state tube and homothetic control tube are sequences of sets $\mathbf{Z}_N := \{Z_k\}_{k\in\mathbb{N}_N}$, and $\mathbf{U}_{N-1} := \{U_k\}_{k\in\mathbb{N}_{N-1}}$. For each relevant time instant k, the sequence of the state and control input are defined as:

$$Z_k := \bar{\mathbf{z}}_k \oplus \alpha_k\mathcal{S}$$
$$U_k := \mathbf{v}_k \oplus \alpha_k\mathcal{R}$$

where $\bar{\mathbf{z}}_k \in \mathbb{R}^n$ denotes the nominal state vector, $\mathbf{v}_k \in \mathbb{R}^m$ denotes the nominal control action vector, and $\alpha_k \in \mathbb{R}_{\geq 0}$ denotes the scaling factor. The control policy is a sequence of control laws $\prod_{N-1} := \pi(\hat{\mathbf{z}}_k, \bar{z}_k, \mathbf{v}_k)_{k\in\mathbb{N}_{N-1}}$, which includes the corrective control to suppress the deviation between the nominal state $\bar{\mathbf{z}}_k$ and the real state $\hat{\mathbf{z}}_k$:

$$\forall\hat{\mathbf{z}}_k \in Z_k, \pi_k(\hat{\mathbf{z}}_k, \bar{z}_k, \mathbf{v}_k)) := K_k(\hat{\mathbf{z}}_k - \bar{\mathbf{z}}_k) + \mathbf{v}_k) \tag{13}$$

According to the theory of HTMPC [19], the necessary conditions are provided as follows:

$$\forall\bar{\mathbf{z}}_k \in \mathbb{Z} \quad \forall k \in \mathbb{N}_{N-1}$$
$$\alpha_k \geq 0$$
$$\bar{\mathbf{z}}_k \in \bar{\mathbf{z}}_0 \oplus \alpha_0\mathcal{S}$$
$$\bar{\mathbf{z}}_k \oplus \alpha_k\mathcal{S} \subseteq \mathbb{Z} \tag{14}$$
$$\mathbf{v}_k \oplus \alpha_k\mathcal{R} \subseteq \mathbb{U} \tag{15}$$
$$\forall(\mathbf{A}_j, \mathbf{B}_j) \in \mathbb{C}, \forall\hat{\mathbf{z}}_k \in \bar{\mathbf{z}}_k \oplus \alpha_k\mathcal{S},$$
$$\{\mathbf{A}_j\hat{\mathbf{z}}_k + \mathbf{B}_j(\mathbf{v}_k + \pi(\cdot))\} \subseteq \bar{\mathbf{z}}_{k+1} \oplus \alpha_{k+1}\mathcal{S} \tag{16}$$
$$\forall\hat{\mathbf{z}}_k \in \bar{\mathbf{z}}_k \oplus \alpha_k\mathcal{S}, K_k(\hat{z}_k - \bar{z}_k) \in \alpha_k\mathcal{R} \tag{17}$$
$$(\bar{\mathbf{z}}_N, \alpha_N) \in G_f \tag{18}$$

where $G_f \subseteq \mathbb{R}^{n+1}$ is a suitable terminal set. From the above conditions, we can speculate that the sequence of tube centers $\{z_k \in \mathbb{R}^n\}$, and $\{v_k \in \mathbb{R}^m\}$, and tube scaling factor $\{\alpha_k \in \mathbb{R}_{\geq 0}\}$ result in the homothetic state tube $\mathbf{Z}_N$, homothetic control tube $\mathbf{U}_{N-1}$ and control policy $\prod_{N-1}$. Then, the decision variable $\mathbf{d}_N := (\bar{\mathbf{z}}_0, \ldots, \bar{\mathbf{z}}_N, v_0, \ldots, v_N, \alpha_0, \ldots, \alpha_N) \in \mathbb{R}^{N(n+m+1)+n+1}$ is introduced into the optimization problem to obtain its feasible solution.

With the decision variable $\mathbf{d}_N$, we define a cost function:

$$\mathrm{V_N}(\mathbf{d}_N) := \sum_{k\in\mathbb{N}_{N-1}} \ell(\bar{\mathbf{z}}_k, \alpha_k, v_l) + \mathrm{V_f}(\bar{\mathbf{z}}_N, \alpha_N) \tag{19}$$

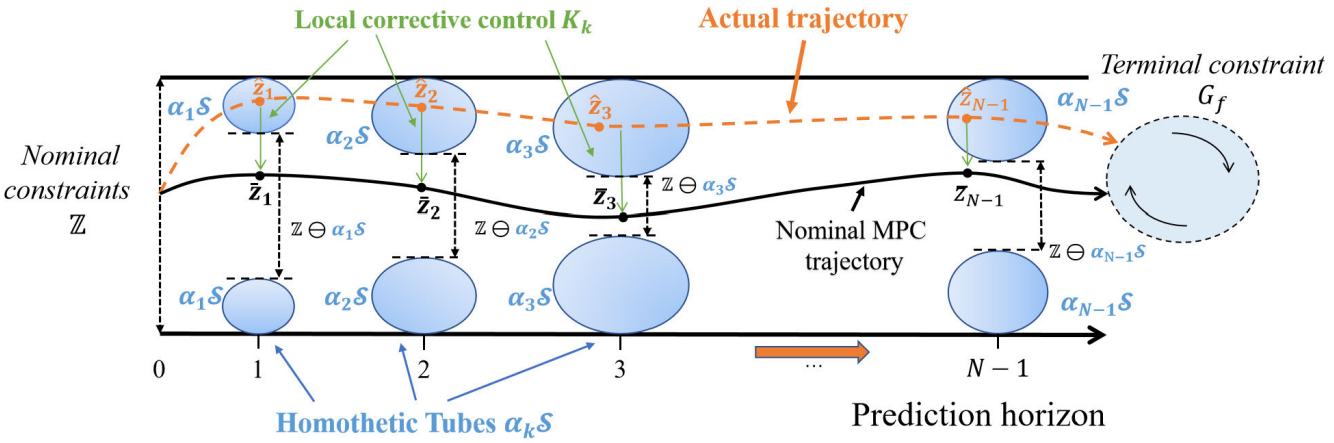

FIGURE 4. Homothetic tube-based MPC strategy. Tubes are resized by homothetic factor α_k; the difference between the actual trajectory and the nominal trajectory is compensated by the corrective control K_k; the optimization problem is based on the tightened constraint $\mathbb{Z} \ominus \alpha_k \mathcal{S}$ to solve the nominal trajectory.

where $\ell(\bar{z}_k, \alpha_k, v_k)$ and $\mathrm{V_f}(\bar{z}_N, \alpha_N)$ are the stage and terminal cost function, respectively. The stage cost function and the terminal cost function are defined as:

$$\ell(\bar{\mathbf{z}}_k, \mathbf{v}_k, \alpha_k) : \bar{\mathbf{z}}_k^T \mathbf{Q} \bar{\mathbf{z}}_k + \mathbf{v}_k^T \mathbf{R} \mathbf{v}_k + \alpha_k^T \mathbf{Q}_\alpha \alpha_k \tag{20}$$

$$\mathrm{V_f}(\bar{\mathbf{z}}_N, \alpha_N) := \bar{\mathbf{z}}_N^T \mathbf{P} \bar{\mathbf{z}}_N + \alpha_N \mathbf{P}_\alpha \alpha_N \tag{21}$$

Remark 4: This paper aims to propose a novel robust tube-based MPC controller by utilizing the established theory of HTMPC. The controller is required to produce an optimal solution under possible parametric uncertainties. The homothetic state tubes $\mathbf{Z}_N$ and control tubes $\mathbf{U}_{N-1}$ could ensure the feasibility by providing less conservative constraints. In the HTMPC framework, we optimize the problem under the worst condition corresponding to the most significant deviations between the nominal state $\bar{\mathbf{z}}$ and actual state $\hat{\mathbf{z}}$. The maximum deviation is associated with the extreme deviation of the model matrices $\mathbf{A_d}$ and $\mathbf{B_d^u}$, such as the matrix pair $(\boldsymbol{A_j}, \boldsymbol{B_j})$. Therefore, we enumerate all vertices of set $\mathbb{C}$ to examine its resulting deviations and minimize the cost function in the worst condition.

B. HOMOTHETIC TUBE-BASED MPC STRATEGY

As the vehicle system entails uncertainties due to the unknown variation of tire cornering stiffness, the future state's predictions could be misleading to cause significant performance loss and instability of the control system. Hence, we consider a homothetic tube-based MPC strategy to produce a sequence of optimal solutions under the worst uncertainty. The process of the HTMPC control framework has been illustrated in Fig. 4. The core of the HTMPC strategy is a min-max optimization problem that minimizes the cost function $\mathbf{V_N}(\mathbf{d_N})$ of the worst case. The worst uncertainty leads to a significant error in the prediction of the controller through the entire receding horizon. By going through all vertices of the matrix pair $(\mathbf{A}_j, \mathbf{B}_j)$, the prediction model $\mathbf{A}_j\hat{\mathbf{z}}_k + \mathbf{B}_j\pi(\cdot)$ produces the nominal state $\hat{\mathbf{z}}_{k+1}$ at the next step that has the largest deviation from its predefined value $\bar{\mathbf{z}}_{k+1}$. We can use the relation in Eq. (16) to transform the upper bound of this deviation to the homothetic tube $\alpha_k\mathcal{S}$ of the error system's state. Thus, the cost term of stage cost in Eq. (20) can describe the influence of the parametric uncertainties. Therefore, the min-max optimization problem minimizes the upper bound of the cost function in Eq. (19) to produce an optimal sequence of decision variables $\mathbf{d_N}$ including the homothetic factor α_k. $\mathbb{Z}$, $\mathbb{U}$ and G_f represent the original constraint of system state, input and terminal state, respectively. This strategy impose a set of more tightened constraints following the relations in Eq. (14-17) such that $\mathbb{Z} \ominus \alpha_k\mathcal{S}$, $\mathbb{U} \ominus \alpha_k\mathcal{R}$, $G_f \ominus \alpha_k\mathcal{S}$. Assume that a measurement of the system state $\hat{\mathbf{z}}$ is available at the current time instant k.

$$\min_{\mathbf{d}_N} \max_{(\mathbf{A}_j, \mathbf{B}_j) \in \mathbb{C}} \{\mathrm{V_N}(\mathbf{d}_N)\} \tag{22}$$

$$\text{s.t. } \bar{\mathbf{z}}_k \in \mathbb{Z} \ominus \alpha_k\mathcal{S} \tag{23}$$

$$\mathbf{v}_k \in \mathbb{U} \ominus \alpha_k\mathcal{R} \tag{24}$$

$$\bar{\mathbf{z}}_N \in G_f \ominus \alpha_k\mathcal{S} \tag{25}$$

$$(\mathbf{A}_j\bar{\mathbf{z}}_k + \mathbf{B}_j\pi_k) \oplus \alpha_k\mathcal{S} \leq \bar{\mathbf{z}}_{k+1} \oplus \alpha_{k+1}\mathcal{S} \tag{26}$$

where $V_N(\mathbf{d}_N)$ and $\mathbf{d}_N$ denote the cost function and decision variable defined in Eq. (19). The decision variables $\mathbf{d}_N$ include z_k, v_k, and α_k representing the predicted state, input, and homothetic factor at current time instant k, respectively. To efficiently solve the optimization problem in Eq. (22), we formulate a recursive online algorithm as follows.

Algorithm 1 (Online Process of HTMPC)

1) At each time instant k, given the known states $\hat{\mathbf{z}}_k$, the action $\mathbf{u}_k$ and the homothetic factor α_k, set the initial value $\bar{\mathbf{z}}_0 = \hat{\mathbf{z}}_k, \mathbf{v}_0 = \mathbf{u}_k, \alpha_0 = \alpha_k$ and then solve the min-max optimization problem in Eq. (22).
2) Use the first element of the solution of the optimization problem, i.e., $\mathbf{v}_1$ and $\bar{\mathbf{z}}_1$ to evaluate the HTMPC control law $\pi_1(\hat{z}_1, \bar{z}_1, \mathbf{v}_1) = \mathbf{v}_1 + K_k(\hat{z}_1 - \bar{z}_1)$.
3) Set $\mathbf{u}(\hat{z}_k) = \pi_1(\cdot)$ and implement the control action $\mathbf{u}(\hat{z}_k)$ to the control system.

In the following subsections, we will present the process of constructing the ellipsoidal tube set and the associated local control law. Then, we will discuss the stability of the HTMPC in subsection.(E).

C. HOMOTHETIC TUBE

As one of the distinctive characteristics of the robust MPC, robust MPC approach can withstand the disturbance caused by uncertainty. Within the context of the HTMPC framework, we divide the control system in Eq. (12) into a nominal system and an error system. We assume to control the nominal system in a disturbance-free environment. The disturbance is assumed to influence the error system.

$$z_{k+1} = \mathbf{A}z_k + \mathbf{B}v_k \tag{27}$$
$$e_{k+1} = \mathbf{A}e_k + \mathbf{B}\rho_k + \mathbf{B^w}w_k \tag{28}$$

where $\mathbf{z_k}$ and $v_\mathbf{k}$ denote the state and the control input sequence of the nominal system. $\mathbf{e_k}$ and $\rho_\mathbf{k}$ denote the error system's state and associated control action. $\mathbf{w_k}$ denotes the disturbance added to the error system.

The disturbance $\mathbf{w_k}$ is related to the state-dependent uncertainty involving the states and control actions of the nominal system. The uncertain component of the nominal system $\Delta\mathbf{A_j z_k}$ and $\Delta\mathbf{B_j}v_\mathbf{k}$ is introduced in Eq. (12). The matrix coefficient $\Delta\mathbf{A_j}$ and $\Delta\mathbf{B_j}$ are given in Eq. (11). Combining the Eq. (11-12), the disturbance w_k is expressed as follows:

$$w_k = \Delta_k(\mathbf{C_y}x_k + \mathbf{D_y^u}v_k) \tag{29}$$

In an uncertain environment, the disturbance w_k occurs to the error system that contributes to the propagation from the current state e_k to the future state e_{k+1} at time step k. Ideally, the state e_k should be bound by the Robust Positively Invariant (RPI) set $\mathcal{E}$ to ensure the asymptotic stability of the error system.

Definition 2 (RPI Set): The set $\mathcal{E}$ is said to be a robust positively invariant set for the error system in Eq. (28) if

$$e_0 \in \mathcal{E} \implies e_k \in \mathcal{E}, \forall w_k \in \mathcal{W}, \forall k \in \mathbb{N}^+ \tag{30}$$

Definition 3 (Minimal RPI Set): The mRPI set $\mathbb{E}$ of the error system is the RPI set in that is contained in every closed RPI set $\mathcal{E}$ of the error system.

To reduce the conservatives of the mRPI set $\mathbb{E}$, we introduce a scaling variable α_k to resize the mRPI set $\mathbb{E}$. Following the above definitions, we can conclude:

$$e_k \in \alpha_k\mathbb{E} \quad \forall k \in \mathbb{N}^+ \tag{31}$$

We apply a feedback control law K_k to the error system to ensure the error state e_k bounded in the mRPI set $\mathbb{E}$. The control law, $\rho_k = -K_k e_k$, contributes to the control action ρ_k. The relation between the control action ρ_k and the mRPI set $\mathbb{E}$ is stated as follows:

$$\rho_k \in \alpha_k(-K_k)\mathbb{E} \tag{32}$$

By combining the state and control action of the nominal system and the error system, the state x_k and control action u_k of the real system could be unified as follow:

$$\begin{aligned} x_k &\doteq z_k \oplus e_k \longrightarrow z_k \oplus \alpha_k\mathbb{E} \\ u_k &\doteq v_k \oplus \rho_k \longrightarrow v_k \oplus (\alpha_k(-K_k)\mathbb{E}) \end{aligned} \tag{33}$$

By normalizing the disturbance w_k to facilitate the mathematical processing, we define a disturbance set $\mathbb{W}$ in the form of the unit set, expressed as

$$\mathbb{W} = \{w \mid w^T w \leq 1\} \tag{34}$$

Combining Eq. (29) and Eq. (34), we define an adjustable disturbance set $\lambda_k\mathbb{Y}$ that bounds the state-dependent disturbance of real system related to its state and control input, expressed as

$$\lambda_k\mathbb{Y} = \{{}^{x_k}_{u_k} | (C_y x_k + D_y^u u_k)^T (C_y x_k + D_y^u u_k) \leq \lambda_k\} \tag{35}$$

From the relation between Eq. (33) and Eq. (35), we can obtain the following relation:

$$\begin{bmatrix} z_k \oplus (\alpha_k\mathbb{E}) \\ v_k \oplus (\alpha_k(-K_R)\mathbb{E}) \end{bmatrix} \subseteq \lambda_k\mathbb{Y} \tag{36}$$

To describe the future state e_{k+1} by the elastic mRPI set $\alpha_{k+1}\mathbb{E}$, we invoke Eq. (28) and conclude a relation between the error state set $\mathbb{E}$ and the disturbance set $\mathbb{Y}$ as follows:

$$(\mathbf{A} - \mathbf{B}K_k)\alpha_k\mathbb{E} \oplus \mathbf{B^w}\lambda_k\mathbb{Y} \subset \alpha_{k+1}\mathbb{E} \tag{37}$$

This relation provides insight into the evolution of the elastic mRPI set $\alpha_{k+1}\mathbb{E}$ under the influence of the disturbance $\lambda_k B_d^w\mathbb{Y}$. We can use this relation to guarantee the stability of the error system in the presence of the disturbance w_k. Therefore, the relation is the necessary component for the constraint of the homothetic tube-based control system, corresponding to Eq. (26).

Remark 4: Direct computation of mRPI set $\mathbb{E}$ for the control system is often infeasible [27]. Then, we utilize the approximate method to substitute the original mRPI set $\mathbb{E}$. The approximate mRPI set is an ellipsoidal set $\mathbf{E} = \{x | x^T \boldsymbol{M} x \leq 1\}$. $\boldsymbol{M}$ denotes the matrix coefficient related to the cross-section of the ellipse. This approximate method is convenient for the mathematical realization of the mRPI set. As the reasoning behind the approximate method is much more complex, we present the critical theorem here. More details can be referred from [38].

Theorem 1 (Approximate Minimal RPI Set): $\mathcal{R}(\sigma)$ is an ellipsoidal approximate minimal robust positively invariant set for the control system subject to a given feedback control law $u_k = K_k x_k$ if there exists $\alpha_\sigma \in [0, 1]$ where the following semi-definite problem has a solution:

$$\inf_{X,Y,\alpha_\alpha,\alpha_\sigma} Tr(X)$$
$$\begin{bmatrix} -X & AX - B^u Y & B^w \\ * & -Xa_\alpha & 0 \\ * & * & -\Upsilon_p \end{bmatrix} \preceq 0$$
$$\forall j \in \mathbb{N}_{1:q} : \begin{bmatrix} -I_{n_{qi}} & \mathbf{C}_{y,j}X - \mathbf{D}^u_{y,j}Y \\ * & -X \end{bmatrix} \preceq 0$$

$$\bar{\alpha} + \sum_{i=1}^{s} a_{\sigma_i} \leq 1 \tag{38}$$

where $\boldsymbol{M} = X^{-1}$, $Y = K_k X$ and Υ_p is the S-Procedure variable. By solving the linear inequality matrix presented in Eq. (38), we can obtain the matrix coefficient $\boldsymbol{M}$ that has the minimum matrix diagonal denoting the minimal volume of the set.

D. CORRECTIVE CONTROL LAW AND TERMINAL COST MATRIX

As an effective robust control technique for the uncertain system, the guarantee-cost control (GCC) produces a state-feedback control law and a cost coefficient to regulate and stabilize the error system in Eq. (28) for compensating the disturbance. We define the quadratic performance index for the error system for all admissible uncertainty as follows:

$$J(N, \Delta\mathbf{A}_\mathbf{e}^\mathbf{l}, \Delta\mathbf{B}_\mathbf{e}^\mathbf{l}) = \sum_{k=0}^{N-1} (\mathbf{e}_k^T \mathbf{Q_G} \mathbf{e}_k + \rho_k^T \mathbf{R_G} \rho_k) \tag{39}$$

where ΔA_e^l, ΔB_e^l denote the uncertainty matrices, which is the l^{th}-vertex on the extreme realization of the uncertainty set $\Delta\mathbf{A}$ and $\Delta\mathbf{B}$. $\mathbf{Q_G}$ and $\mathbf{R_G}$ are the predefined cost matrices on state and control action, respectively. To present this method, we utilize three theorems proposed in the previous related research [40]. The proof of the theorems can be found in the publications [39], [40], and we will concentrate on the specific application of the GCC method.

Theorem 2: For a control system in Eq. (12) with the cost function in Eq. (39), the closed-loop control system is asymptotically stable if there exists a feedback control law $u_k = \mathbf{K_k} x_k$ and a positive definite cost matrix $\mathbf{P}$ satisfying the matrix inequality

$$\hat{A}_k^T \mathbf{P} + \mathbf{P}\hat{A}_k + K_k^T R_G K_k + Q_G \prec 0 \tag{40}$$

where $\hat{A}_k = A_d + B_d^u K_k + B_d^w \Delta_k (\Delta C_y + \Delta D_y^u K_k)$. By using the control law $u_k = \mathbf{K_k} x_k$, the closed-loop system could achieve to such a performance index for all admissible uncertainties as follows:

$$J(N, \Delta A_e^l, \Delta B_e^l) < e_0^T \mathbf{P} e_0, \quad e_0 \neq 0 \tag{41}$$

where $e_0^T \mathbf{P} e_0$ denotes the guaranteed cost for the uncertain system. We need to obtain a feasible solution of matrix $\mathbf{P}$ with the minimum eigenvalues to minimize the bound of guaranteed cost.

Theorem 3: For the closed-loop system, there exists matrix $\mathbf{P} = \mathbf{P}^T > 0$ and the feedback gain K_k such that the linear matrix inequality in Eq. (40) holds if and only if there exist scalar $\delta > 0$ and matrix X and Y, such that the following condition is satisfied as

$$\begin{bmatrix} A_k & B_k^T & X & Y^T \\ B_k & -\delta I & 0 & 0 \\ X & 0 & -Q_G^{-1} & 0 \\ Y & 0 & 0 & -R_G^{-1} \end{bmatrix} \leq 0 \tag{42}$$

where $A_k = AX + B^u Y + (AX + B^u Y)^T + \delta B^w (B^w)^T$. $B_k = \Delta C_y X + \Delta D_y^u Y$. Taking the Schur complement to transform the condition in Eq. (40) into the linear inequalities, the inequality in Eq. (42) is obtained with homogeneous transformations $X = \mathbf{P}^{-1}$ and setting $Y = K_k \mathbf{P}^{-1}$. If the matrix inequality in Eq. (42) has a feasible solution (δ, X, Y), the cost matrix $\mathbf{P}$ and the feedback gain K_k can be obtained by $\mathbf{P} = X^{-1}$ and $K_k = Y X^{-1}$.

Theorem 4: For the uncertain control system in Eq. (12) with the cost function in Eq. (39), $u_k = Y X^{-1} x_k$ is an optimal state feedback control law, if there exists a solution (δ, X, Y, S) for the optimization problem give by:

$$\begin{aligned} &\min_{\delta, X, Y, S} \quad \mathrm{Tr}(S) \\ &\text{s.t. } (i) \begin{bmatrix} A_k & B_k^T & X & Y^T \\ B_k & -\delta I & 0 & 0 \\ X & 0 & -Q_G^{-1} & 0 \\ Y & 0 & 0 & -R_G^{-1} \end{bmatrix} \leq 0 \\ &\quad (ii) \begin{bmatrix} S & I \\ I & X \end{bmatrix} \geq 0 \end{aligned} \tag{43}$$

As a result of the minimization of the problem in Eq. (43), the problem's solution (δ, X, Y, S) can determine the cost matrix $\boldsymbol{P} = X^{-1}$ and the control gain $K_k = YX^{-1}$. Taking the Schur Complement, the constraint (ii) of the Eq. (43) is equivalent to $S > X^{-1} > 0$; then, the minimum of $\mathrm{Tr}(S)$ can ensure the minimum of the eigenvalue of the cost matrix $\mathbf{P}$. The control law gain K_k calculated by the corrective control algorithm could be applied in Eq. (13) to complement the actual control action. The matrix $\mathbf{P}$ will be applied as the weighting coefficient of terminal cost in Eq. (21).

E. ANALYSIS OF STABILITY

In this section, we discuss the stability property of the proposed HTMPC controller. The proposed controller with terminal cost $V_f(z_N, \alpha_N)$ and terminal region constraint G_f can asymptotically stabilize the uncertain system. Sufficient conditions over $V_f(\bullet)$ and G_f are necessary to guarantee stability and are presented as follows:

1) The terminal region constraint G_f must be an admissible robust positive invariant set of the system.
2) The terminal cost function $V_f(\bullet)$ is a Lyapunov function of the closed-loop system that is regulated by the local controller $u = \bar{u} + K(z - \bar{z})$. The condition for the terminal cost function is presented as:

$$V_f(A_k z_k) + \ell(z_k, K z_k) \leq V_f(z_k) \; \forall z_k \in G_f \tag{44}$$

The terminal cost function can guarantee that the optimized cost is strictly decreasing. In this scenario, the difference between the cost function of $V_N^0(Az_k + B\kappa_N^0)$ and the previously optimized cost $V_N^0(z_k)$ for the optimization problem is presented as follows:

$$\begin{aligned} V_N^0(Az_k + B\kappa_N^0) - V_N^0(z_k) = &-\ell(z_k) + \ell(Az_k + B\kappa_N^0, \kappa_N^0) \\ &+ V_f(Az_k + B\kappa_N^0) - V_f(z_k) \end{aligned} \tag{45}$$

TABLE 2. Vehicle and road parameters for simulation.

Symbol	Definition	Values (Unit)
m	Vehicle mass	1590 (kg)
I_z	Yaw moment of inertia	2687 (kg $\cdot$ m^2)
l_f	Distance of CG from front axle	1.18(m)
l_r	Distance of CG from rear axle	1.77(m)
l	Wheelbase	2.95 (m)
C_{f0}	Nominal cornering stiffness of front tire	7.5 (KN/rad)
C_{r0}	Nominal cornering stiffness of rear tire	8.5 (KN/rad)
ΔC_f	Variation bound of front tire cornering stiffness	4 (KN/rad)
ΔC_r	Variation bound of rear tire cornering stiffness	4 (KN/rad)
Δt_s	Model discretized step	0.05 (s)
H_p	Prediction horizon	15
H_c	Control horizon	5
Q_α	Cost weight on scaling factor	1000
ρ_ϵ	Cost weight on slack variable	1000
$\|e_{\Delta y}\|$	constraint bound on lateral error	0.5 (m)
$\|e_{\Delta\psi}\|$	constraint bound on heading error	0.2 (rad)
$\|\delta_f\|$	constraint bound on control input	0.4(rad)
$\hat{\varepsilon}_X$	Noise variance on Location X^{CG}	0.05 (m)
$\hat{\varepsilon}_Y$	Noise variance on Location Y^{CG}	0.05 (m)
$\hat{\varepsilon}_\psi$	Noise variance on Yaw angle ψ	1°
$\hat{\varepsilon}_{v_x}$	Noise variance on longitudinal velocity v_x	0.05 (m/s)
$\hat{\varepsilon}_{v_y}$	Noise variance on lateral velocity v_y	0.05 (m/s)
$\hat{\varepsilon}_\omega$	Noise variance on yaw rate ω	1°/s

With condition in Eq. (44), the second term in the summation in Eq. (45) is guaranteed to be non-positive, so the feasible cost function has a lower cost than the previous optimized function. According to the principle of optimality, the overall cost $V_N^0(z_{k+1})$ will also have a lower cost than the previously optimized $V_N^0(z_k)$. Then, the new condition is given by:

$$V_N^0(z_{k+1}) - V_N^0(z_k) \leq -J(z_k, u_k)$$

where the optimized cost $V_N^0(z_k)$ represents a function of Lyapunov that decreases throughout the evolution of the nominal system, which guarantees the asymptotic stability of the system.

F. CONTROLLER PARAMETER CALCULATION

The nominal configurations of the vehicle and control framework are listed in Table 2. By solving the optimization problems in Eq. (42-43), we can obtain the solution X, Y of the optimal problem, which determines the local control feedback gain K_k and terminal cost matrix $\mathbf{P}$. We can solve the LMI-based optimization problem in Eq. (38) by substituting the feedback gain K_k into this formulation. The solution to this problem, X, is equivalent to the matrix coefficient M representing the cross-section of the approximate ellipsoidal tube shape set $\mathbb{E}$. Subsequently, the above controller parameters, including the feedback gain K_k, the homothetic tube shape set $\mathbb{E}$, and the terminal cost coefficient $\mathbf{P}$, lead to the solution of the optimization problem in Eq. (22-26). For simplicity, we directly present the feedback law K_k, the terminal cost coefficient $\mathbf{P}$, and the matrix coefficient M as follows:

$$K_k = \begin{bmatrix} 1.8351 & 2.3578 & 0.2447 & 0.1046 \end{bmatrix}$$

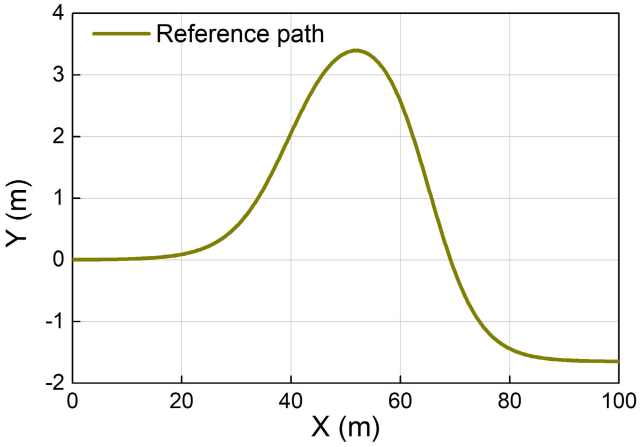

FIGURE 5. The reference trajectory of the double lane change maneuver, starting from $X = 0$ and ending at $X = 100$. The vehicle is tracking the reference trajectory at the constant speed.

$$\mathbf{P} = \begin{bmatrix} 329.78 & 185.08 & 28.79 & -0.23 \\ 185.08 & 9793.49 & 39.14 & 43.67 \\ 28.89 & 39.14 & 7.53 & -0.16 \\ -0.23 & 43.67 & -0.16 & 6.39 \end{bmatrix}$$

$$M = \begin{bmatrix} 0.0067 & -0.0065 & -0.0004 & -0.0091 \\ -0.0065 & 0.0122 & 0.0103 & 0.0003 \\ -0.0004 & 0.0103 & 0.4861 & -0.0716 \\ -0.0091 & 0.0003 & -0.0716 & 0.9137 \end{bmatrix}$$

IV. FRAMEWORK FOR ROBUST PERFORMANCE COMPARISON

We construct a driving environment in the professional vehicle simulation software CARSIM. The platform allows us to adjust road conditions to simulate the actual road closely, including adhesion coefficient, road elevation, and surface roughness. We simulate a high-fidelity D-class SUV model in the typical double lane change (DLC) maneuver. The parameters for the reference path are provided in Table 2. DLC is typically an emergency avoidance maneuver, shown in Fig. 5. In the ideal condition, vehicle is controlled to track the reference trajectory with slight deviation. However, the uncertain disturbance would cause sharply increasing deviation. The tracking offset would demonstrate the controller's ability to reject the disturbance and enhance the vehicle's lateral dynamics capacity to complete the DLC maneuver. In this way, we can test the controllers when tracking this DLC trajectory subjected to unknown disturbances. We perform various tests to evaluate the robustness of the controllers against low road adhesion, measurement noise, and parametric uncertainties due to random road friction. We conduct the Monte Carlo simulations in the last two tests. In order to obtain a quantitative evaluation of the robust performance of different controllers, we use the following measures to compare the tracking performance according to the lateral deviation of the CG of vehicle (X^{CG}, Y^{CG}) to the target point of path $(X(t), Y(t))$ as e_y:

1) maximum tracking error: $\max_{t\in[0,T]} |e_y|$
2) average cumulative tracking error: $\frac{1}{T}\int_0^T |e_y| dt$

In this section, the three tests are considered and run on these controllers. These tests include:

1) Normal and low road adhesion coefficient: We simulate the two road conditions, including the standard friction coefficient as 0.85 and the low friction coefficient as 0.6.
2) Measurement noise: White Gaussian noise is added to the state of the vehicle system to model measurement noise. The vector $[X^{CG}, Y^{CG}, \psi, v_x, v_y, \omega]$ is 'measured'; and the variance of each dimension of the error process is selected as $\sigma_i = \hat{\varepsilon}$. The value of ε is given in Table 2.
3) Uncertain friction coefficient: The uncertain road friction condition simulates the typical situation on a snow-ice track, where the surface condition constantly changes for a normal distribution over [0.4 0.8] and changes every 0.1 seconds.

In this paper, we compare the robustness of four controllers, including the proposed control algorithm and robust control techniques studied by other researchers. The first controller utilizes the homothetic model predictive control algorithm proposed in Section III. The second controller is a tube-based model predictive control (TMPC), which calculates the maximal robust positive invariant(MRPI) set for the control system when the external disturbances occur. Like the HTMPC, TMPC also uses feedback control to compensate for the error between the nominal and actual systems. The third controller is a deterministic MPC controller, which is not equipped with any robust control component. The last one is based on a robust control algorithm, the Immersion and Invariance Principle (I&I). The I&I controller is resilient to parametric uncertainties and external disturbances. Furthermore, all simulations ran on a desktop computer (i5 2.8GHz, 8GB RAM) and were implemented in co-simulation platform of Matlab and Carsim using the Simulink software together with the Gurobi solver. The simulation scripts have been made available at https://github.com/HuKangle/Trajectory-tracking-for-vehicle.git.

V. RESULTS AND DISCUSSION

In this section, we present the results of the selected test cases. We evaluate the controllers from the following aspects: the standard deviation of lateral tracking errors, maximum lateral tracking error, and the control action of different controllers. Besides, the result of the homothetic factor α could illustrate the mechanism of the proposed HTMPC algorithm.

A. NORMAL AND LOW ROAD ADHESION SCENARIO

The purpose of this test is to determine whether the controllers are robust against low road coefficient. Fig. 6(a) illustrates the tire cornering stiffness of the front tire and rear tire in normal road friction and low road friction, respectively. We utilize a recursive least square (RLS) algorithm to give

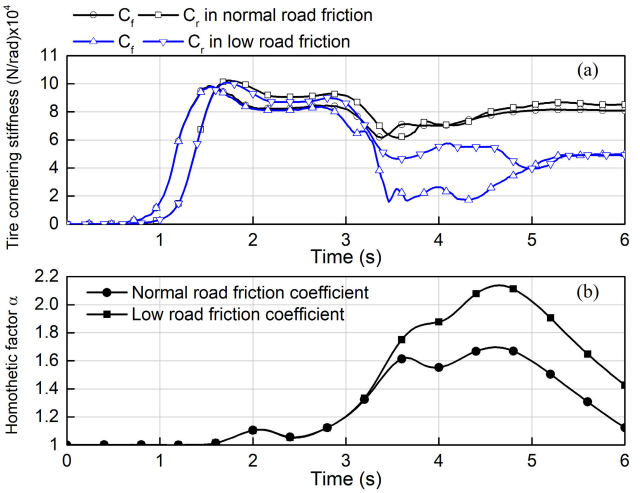

FIGURE 6. The tire cornering stiffness and the resulting homothetic factor of the proposed controller in the normal and low road friction coefficients, respectively: (a) the front and rear tire cornering stiffness C_f, C_r in the standard friction coefficient and low friction coefficient, respectively; (b) the homothetic factor α in the normal friction coefficient and the low friction coefficient.

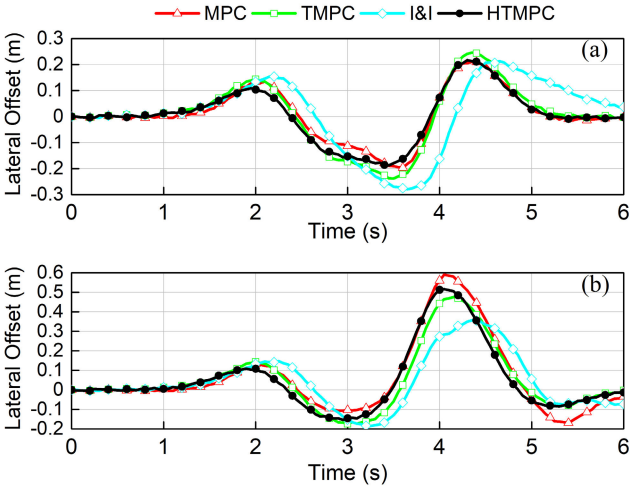

FIGURE 7. The trajectory tracking error of the controllers in the scenario of the standard and low road friction coefficient: (a) the tracking errors under the condition of the standard friction coefficient; (b) the tracking errors under the condition of the low friction coefficient.

a rough estimate of the tire cornering stiffness. From the changing trend of the tire cornering stiffness in different road friction, we can infer that the variations of both tire cornering stiffness are associated with the varying friction coefficient. As the vehicle begins a drastic steer around 3 seconds, the difference in the tire cornering stiffness increases significantly. However, the difference gradually decreases as the vehicle drives to the target lane. This changing trend suggests that variations of tire cornering stiffness are closely related to the state and input of the vehicle. The apparent deviation, therefore, leads to state-dependent uncertainties of tire cornering stiffness that could result in a mismatch between the nominal system and the actual system of the vehicle path tracking.

The proposed HTMPC controller can include this state-dependent uncertainty in the control framework. On the one

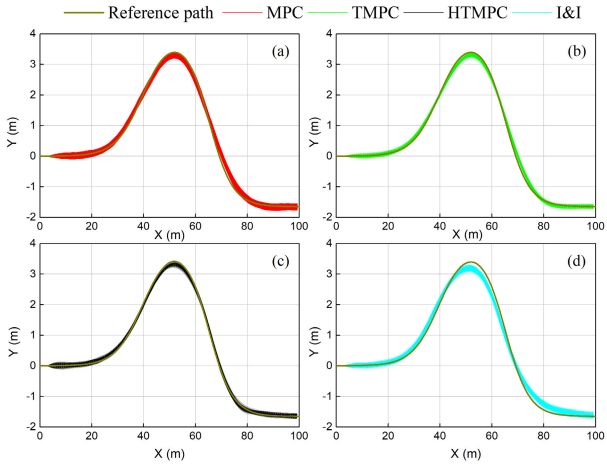

FIGURE 8. The trajectories of different controllers in the Monte-Carlo simulation regarding the measurement noise: (a) MPC; (b) TMPC; (c) HTMPC; (d) I&I.

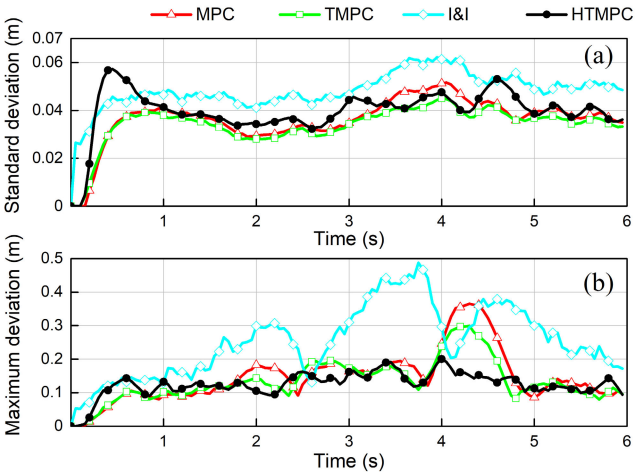

FIGURE 9. The comparison of the robustness of different controllers using Monte Carlo simulation regarding the measurement noise: (a) standard deviation of error; (b) Maximum error.

hand, it constructs the min-max optimization problem based on the extreme value of the cornering stiffness. This framework enables the controller to produce a feasible solution to the problem under the worst condition. On the other hand, the controller utilizes the homothetic factor α to stretch the "tube" and bound the increasing disturbance caused by the state-dependent uncertainties. Fig. 6(b) illustrates the homothetic factor α at different road friction coefficients. The homothetic factor α increases mildly for a slight decline of tire cornering stiffness in the normal condition. In contrast, the factor α increases rapidly for the dramatic reduction of tire cornering stiffness in the low friction condition. The constraints of system state and input are tightened by an enlarged "tube" following Eq. (14-15), which could ensure the constraint satisfaction and the feasibility of the optimization problem. On the contrary, the deterministic MPC controller depends on the constant cornering stiffness of the tire, so the controller cannot adapt to the changing tire cornering stiffness caused by low road friction.

Fig. 7 illustrates the controllers' tracking offset in the conditions of the standard and low road adhesion, respectively. All controllers produce similar tracking errors in normal conditions. In the low adhesion condition, HTMPC and TMPC controllers perform well in rejecting the disturbance so that their tracking errors are more minor than that of deterministic MPC controller. I&I controller produces the lowest tracking error in the low road adhesion, suggesting its robustness to deal with the uncertainty. The result of the low road adhesion scenario illustrates the improvement of the HTMPC controller relative to the deterministic MPC controller. Further, we will compare the HTMPC controller with TMPC and I&I controllers regarding their robustness to the unknown disturbance and uncertainty in the following subsections.

B. MEASUREMENT NOISE

In this case, we test the robust performance of the controllers due to sensor noise using Monte Carlo simulation. We evaluate the robustness of the controllers from two aspects: the standard deviation of the tracking error and the maximum error. The standard deviation of the tracking error can be used to assess the robustness of the controllers through its ability to quantify the distribution of the random trajectory. The maximum position error indicates the controller's ability to suppress the most severe disturbance. This index is critical in evasive maneuvers since minimized tracking errors are necessary to guarantee collision avoidance. As the measurement noise is unknown to the vehicle system, the controllers produce the randomly distributed trajectories, shown in Fig. 8. Fig. 9(a) shows the standard deviation of the tracking errors of all controllers. At the beginning of maneuver, HTMPC exhibits an overshoot of the standard deviation of tracking error, which demonstrates the drawbacks of HTMPC to suppress the noise at the beginning. Nonetheless, HTMPC could adjust the homothetic factor α_k to enhance the robustness to the noise and then behaves similarly to other optimal controllers. Besides, I&I controller produces a higher standard deviation through the whole maneuver, indicating that the I&I controller is highly influenced by noise. Meanwhile, as shown in Fig. 9(b), the I&I controller causes more significant fluctuations in the maximum tracking error. The I&I controller behaves less robustly than model-based controllers under noise. Fig. 9(b) also illustrates that MPC and TMPC controllers display an increase in the maximum tracking deviation between 4 s and 5 s corresponding to a rapidly changing path. The vehicle violently steers to track this path segment, intensifying the disturbance caused by measurement noise. The TMPC controller achieves a slightly lower maximum error than the MPC controllers, while the HTMPC controller produces a much lower maximum tracking error than both MPC and TMPC controllers. This difference indicates that the HTMPC controller has a more effective and robust mechanism to suppress the noise. Comparing both evaluation metrics indicates that the proposed HTMPC could maintain strong robustness in the presence of measurement noise.

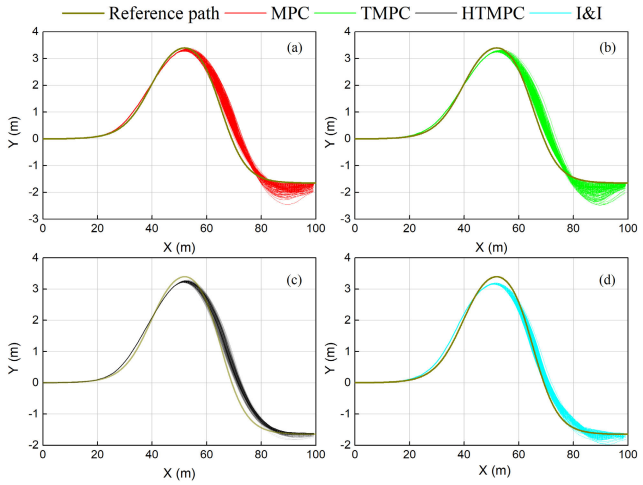

FIGURE 10. The trajectories of different controllers in the Monte-Carlo analysis regarding the uncertain road friction coefficient: (a) MPC; (b) TMPC; (c) HTMPC; (d) I&I.

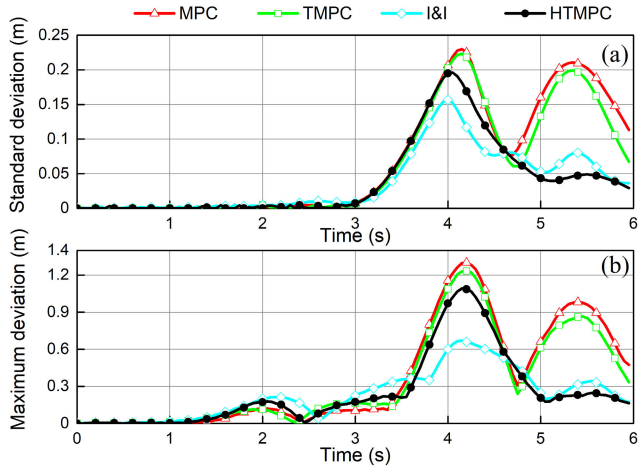

FIGURE 11. The comparison of the robustness of different controllers using Monte Carlo simulation regarding the uncertain road friction coefficient: (a) standard deviation of error; (b) Maximum error.

C. UNCERTAIN ROAD ADHESION

In this case, we test the robustness of the controllers when the tire-road adhesion is unpredictable and constantly changing. As shown in Fig. 10, compared to the tight trajectory in the scenario of measurement noise in Fig. 8, all controllers produce a wider distribution of tracking trajectory in the scenario of random road friction. This difference indicates that random road friction causes more disturbances than the measurement noise. Because the random friction dramatically changes the tire cornering stiffness, which magnifies the model mismatch when the vehicle is conducting intense driving. Therefore, we can observe a significant tracking deviation and tracking overshoot in the second half of the trajectory.

We use the standard deviation and the maximum of the tracking error derived from the trajectory in Fig. 10 to evaluate the robustness of the controller. Fig. 11 shows all controllers' standard deviation and maximum tracking error,

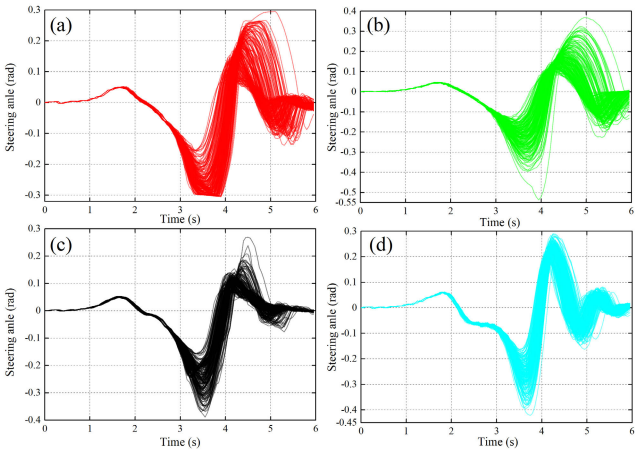

FIGURE 12. The comparison of the control action of different controllers in Monte Carlo simulations regarding the uncertain road friction coefficient: (a) MPC; (b) TMPC; (c) HTMPC; (d) I&I.

respectively. Both indicators of all controllers follow the same trend: two peaks corresponding to the maximum trajectory deviation and overshoot. As shown in Fig. 11, the HTMPC controller produces a similar level of both indicators compared to MPC and TMPC controllers at the first peak. The HTMPC controller provides the lowest level of both indicators at the second peak. Meanwhile, MPC and TMPC controllers exhibit a sharp increase in both indicators. Besides, compared with the I&I controller, the HTMPC controller produces a higher peak at first and then a similar peak of both indicators. Different results in Fig. 11 indicate that the HTMPC controller is as robust as the I&I controller, while both controllers are more robust than the MPC and TMPC controllers.

The advantage of the HTMPC controller is twofold: (a) optimizing the tube geometry according to the uncertainty; (b) adopting the corrective control action to deal with the model mismatch. As the HTMPC controller counteracts the deteriorating uncertainty at the first peak, the controller enlarges the tube to tighten the constraints and provides an aggressive control action. With the uncertainty decreasing afterward, the tube is resized to relax the constraints, and the control action is decreased subsequently with a less corrective component. In this way, as shown in Fig. 12(c), the control action of the HTMPC controller increases near the limit and shrinks to a low level after 4 seconds. Although the control actions of the other controllers are also aggressive close to 4 seconds, MPC and TMPC controllers still provide an unnecessary substantial control action, as shown in Fig. 12(a-b). Therefore, MPC and TMPC cause the prominent trajectory overshoot because of this improper control input, irrespective of the decreasing disturbance.

D. AVERAGE CUMULATIVE-ERROR-BASED SCORING

In this subsection, we displays the scores of different algorithms in each scenarios. The mean of cumulative tracking

TABLE 3. Scores of all controllers on the average cumulative tracking error.

Controller	Low Road Friction	Measurement Noise	Parametric Uncertainties
MPC	1.39	1.53	1.2
TMPC	1.11	1.37	1.25
HTMPC	1.15	1	1.12
I&I	1	2.56	1

errors in the corresponding simulation scenarios determines the score. A sequence of the average of all cumulative tracking errors constitutes the vector C_{comb}. The score s_i of the controllers is defined by: $s_i = \frac{C_{cumu,i}}{min(C_{comb})}$. In this manner, for each control algorithm, the controller with the lowest error is given a score of 1; the lowest errors normalize the errors of other controllers.

Table.3 presents the score of controllers in three scenarios. The scores of the HTMPC and TMPC are superior to MPC in all scenarios. Both robust controllers employ corrective feedback control to resist the disturbances. Whereas TMPC still performs behind the HTMPC in two scenarios of parametric uncertainty. The reason is that TMPC relies on the predefined fixed tube so that TMPC cannot bind the disturbance out of the preset range. HTMPC controller performs better than the I&I control in the case of measurement noise, while both controllers present similar robustness in other cases. The HTMPC controller has strong robustness to measurement noise, while measurement noise badly misleads the I&I controller. Based on the results, we conclude that the HTMPC provides comprehensive robustness under various scenarios.

VI. CONCLUSION

In this work, a homothetic tube-based MPC (HTMPC) strategy has been developed and validated on a front-steer vehicle tracking a double-lane-change trajectory. The proposed strategy aims to compensate for the model mismatch and improve the tracking system's robust performance. We develop a dynamical path tracking model combining the lateral dynamics of the vehicle and simplified tire dynamics considering the uncertainty of tire cornering stiffness. The HTMPC scheme ensures the robustness of the tracking system under worst-case uncertainty by optimizing an online min-max problem that minimizes the upper bound of the cost function for all realizations of extreme uncertainty. Also, we use some effective methods to complement the strategy, including the guaranteed-cost control method and the homothetic tube method. The former decides the terminal cost weighting matrix and the local control law. The latter chooses an approximate tube based on the homothetic factor evolution equation considering the bound of state-dependent disturbances.

The Monte-Carlo simulation results are analyzed based on specific methodologies and metrics to evaluate the robustness of the proposed strategy. Based on the qualitative analysis, the HTMPC controller outperforms the I&I controller in the presence of measurement noise, and it provides better robustness under parametric uncertainty compared to MPC and TMPC. In the scenario of measurement noise, HTMPC produces the lowest cumulative tracking errors; likewise, HTMPC achieves a similar level of tracking error as I&I considering random road friction. Therefore, HTMPC controller offers a higher level of robustness than deterministic MPC and TMPC controllers and is comparable to the I&I control.

The advantage of the HTMPC is to employ the homothetic factor to dynamically resize the tube to reduce the conservative performance of TMPC that depends on the fixed tube. Nevertheless, the HTMPC algorithm only considers the extreme realizations of the parametric uncertainty. To obtain accurate predictions of the bounds of varying parameters, HTMPC could integrate the Dual Extended Kalman Filter, widely used for vehicle state and parameter estimation.

REFERENCES

[1] R. E. Precup and S. Preitl, "Stability and sensitivity analysis of fuzzy control systems. Mechatronics applications," *Acta Polytechnica Hungarica*, vol. 3, no. 1, pp. 61–76, 2006.
[2] T. D. Do, H. H. Choi, and J.-W. Jung, "SDRE-based near optimal control system design for PM synchronous motor," *IEEE Trans. Ind. Electron.*, vol. 59, no. 11, pp. 4063–4074, Nov. 2012.
[3] L. Zhang, H. Ding, J. Shi, Y. Huang, H. Chen, K. Guo, and Q. Li, "An adaptive backstepping sliding mode controller to improve vehicle maneuverability and stability via torque vectoring control," *IEEE Trans. Veh. Technol.*, vol. 69, no. 3, pp. 2598–2612, Mar. 2020.
[4] S. Fergani, L. Menhour, O. Sename, L. Dugard, and B. D'Andréa-Novel, "Integrated vehicle control through the coordination of longitudinal/lateral and vertical dynamics controllers: Flatness and LPV/H_∞-based design," *Int. J. Robust Nonlinear Control*, vol. 27, no. 18, pp. 4992–5007, Dec. 2017.
[5] G. Tagne, R. Talj, and A. Charara, "Design and validation of a robust immersion and invariance controller for the lateral dynamics of intelligent vehicles," *Control Eng. Pract.*, vol. 40, pp. 81–92, Jul. 2015.
[6] F. M. Barbosa, L. B. Marcos, M. M. da Silva, M. H. Terra, and V. Grassi, "Robust path-following control for articulated heavy-duty vehicles," *Control Eng. Pract.*, vol. 85, pp. 246–256, Apr. 2019.
[7] I. A. Zamfirache, R.-E. Precup, R.-C. Roman, and E. M. Petriu, "Policy iteration reinforcement learning-based control using a grey wolf optimizer algorithm," *Inf. Sci.*, vol. 585, pp. 162–175, Mar. 2022.
[8] Y. Chen, C. Hu, Y. Qin, M. Li, and X. Song, "Path planning and robust fuzzy output-feedback control for unmanned ground vehicles with obstacle avoidance," *Proc. Inst. Mech. Engineers, D, J. Automobile Eng.*, vol. 235, no. 4, pp. 933–944, Mar. 2021.
[9] B. Kouvaritakis and M. Cannon, "Developments in robust and stochastic predictive control in the presence of uncertainty," *ASCE-ASME J. Risk Uncertainty Eng. Syst., B, Mech. Eng.*, vol. 1, no. 2, Jun. 2015.
[10] A. Bemporad, F. Borrelli, and M. Morari, "Min-max control of constrained uncertain discrete-time linear systems," *IEEE Trans. Autom. Control*, vol. 48, no. 9, pp. 1600–1606, Sep. 2003.
[11] H. Peng, W. Wang, Q. An, C. Xiang, and L. Li, "Path tracking and direct yaw moment coordinated control based on robust MPC with the finite time horizon for autonomous independent-drive vehicles," *IEEE Trans. Veh. Technol.*, vol. 69, no. 6, pp. 6053–6066, Jun. 2020.
[12] S. Mata, A. Zubizarreta, and C. Pinto, "Robust tube-based model predictive control for lateral path tracking," *IEEE Trans. Intell. Vehicles*, vol. 4, no. 4, pp. 569–577, Dec. 2019.
[13] J. Yu, X. Guo, X. Pei, Z. Chen, and W. Zhou, "Path tracking control based on tube MPC and time delay motion prediction," *IET Intell. Transp. Syst.*, vol. 14, no. 1, pp. 1–12, Jan. 2020.
[14] C. E. Beal and J. C. Gerdes, "Model predictive control for vehicle stabilization at the limits of handling," *IEEE Trans. Control Syst. Technol.*, vol. 21, no. 4, pp. 1258–1269, Jul. 2013.

[15] W. Wang, Y. Zhang, C. Yang, T. Qie, and M. Ma, "Adaptive model predictive control-based path following control for four-wheel independent drive automated vehicles," *IEEE Trans. Intell. Transp. Syst.*, vol. 23, no. 9, pp. 14399–14412, Sep. 2022.
[16] C. Sun, H. Dong, X. Zhang, and C. Geng, "Path tracking controller design for autonomous vehicle based on robust tube MPC," *Int. J. Vehicle Des.*, vol. 82, no. 1, pp. 120–139, Apr. 2020.
[17] B. T. Lopez, J.-J.-E. Slotine, and J. P. How, "Dynamic tube MPC for nonlinear systems," in *Proc. Amer. Control Conf. (ACC)*, Philadelphia, PA, USA, Jul. 2019, pp. 1655–1662.
[18] S. V. Raković, B. Kouvaritakis, R. Findeisen, and M. Cannon, "Homothetic tube model predictive control," *Automatica*, vol. 48, no. 8, pp. 1631–1638, Aug. 2012.
[19] S. V. Rakovic and Q. Cheng, "Homothetic tube MPC for constrained linear difference inclusions," in *Proc. Control Decis. Conf. (CCDC)*, May 2013, pp. 754–761.
[20] S. V. Rakovic, W. S. Levine, and B. Acikmese, "Elastic tube model predictive control," in *Proc. Amer. Control Conf. (ACC)*, Boston, MA, USA, Jul. 2016, pp. 3594–3599.
[21] W. Langson, I. Chryssochoos, S. V. Raković, and D. Q. Mayne, "Robust model predictive control using tubes," *Automatica*, vol. 40, no. 1, pp. 125–133, 2004.
[22] S. V. Rakovic, B. Kouvaritakis, M. Cannon, C. Panos, and R. Findeisen, "Parameterized tube model predictive control," *IEEE Trans. Autom. Control*, vol. 57, no. 11, pp. 2746–2761, Nov. 2012.
[23] R. Heydari and M. Farrokhi, "Robust tube-based model predictive control of LPV systems subject to adjustable additive disturbance set," *Automatica*, vol. 129, Jul. 2021, Art. no. 109672.
[24] J. Hanema, M. Lazar, and R. Tóth, "Heterogeneously parameterized tube model predictive control for LPV systems," *Automatica*, vol. 111, Jan. 2020, Art. no. 108622.
[25] Z. Dong and D. Angeli, "Homothetic tube-based robust economic MPC with integrated moving horizon estimation," *IEEE Trans. Autom. Control*, vol. 66, no. 1, pp. 64–75, Jan. 2021.
[26] Y. Kim, X. Zhang, J. Guanetti, and F. Borrelli, "Robust model predictive control with adjustable uncertainty sets," in *Proc. IEEE Conf. Decis. Control*, Dec. 2018, pp. 5176–5181.
[27] S. V. Rakovic, E. C. Kerrigan, K. I. Kouramas, and D. Q. Mayne, "Invariant approximations of the minimal robust positively invariant set," *IEEE Trans. Autom. Control*, vol. 50, no. 3, pp. 406–410, Mar. 2005.
[28] Y. Gao, A. Gray, H. E. Tseng, and F. Borrelli, "A tube-based robust nonlinear predictive control approach to semiautonomous ground vehicles," *Veh. Syst. Dyn.*, vol. 52, no. 6, pp. 802–823, Jun. 2014.
[29] W. Yang, D. Xu, B. Jiang, and P. Shi, "A novel dual-mode robust model predictive control approach via alternating optimizations," *Automatica*, vol. 133, Nov. 2021, Art. no. 109857.
[30] M. E. Villanueva, R. Quirynen, M. Diehl, B. Chachuat, and B. Houska, "Robust MPC via min–max differential inequalities," *Automatica*, vol. 77, pp. 311–321, Mar. 2017.
[31] R. Gonzalez, M. Fiacchini, T. Alamo, J. L. Guzman, and F. Rodriguez, "Adaptive control for a mobile robot under slip conditions using an LMI-based approach," *Eur. J. Control*, vol. 16, no. 2, pp. 144–155, 2010.
[32] D. V. Balandin and M. M. Kogan, "Control and estimation in linear time-varying systems based on ellipsoidal reachability sets," *Automat. Remote Control*, vol. 81, pp. 1367–1384, Sep. 2020.
[33] L. Xu, W. Zhuang, G. Yin, G. Li, and C. Bian, "Robust overtaking control of autonomous electric vehicle with parameter uncertainties," *Proc. Inst. Mech. Eng., D, J. Automobile Eng.*, vol. 233, no. 13, pp. 3358–3376, Nov. 2019.
[34] Y. I. Lee, B. Kouvaritakis, and M. Cannon, "Constrained receding horizon predictive control for nonlinear systems," *Automatica*, vol. 38, no. 12, pp. 2093–2102, Dec. 2002.
[35] M. Cannon, J. Buerger, B. Kouvaritakis, and S. Rakovic, "Robust tubes in nonlinear model predictive control," *IEEE Trans. Autom. Control*, vol. 56, no. 8, pp. 1942–1947, Aug. 2011.
[36] B. Houska, A. Mohammadi, and M. Diehl, "A short note on constrained linear control systems with multiplicative ellipsoidal uncertainty," *IEEE Trans. Autom. Control*, vol. 61, no. 12, pp. 4106–4111, Dec. 2016.
[37] D. Calzolari, B. Schurmann, and M. Althoff, "Comparison of trajectory tracking controllers for autonomous vehicles," in *Proc. IEEE 20th Int. Conf. Intell. Transp. Syst. (ITSC)*, Yokohama, Japan, Oct. 2017, pp. 1–8.
[38] C. M. Massera, T. C. dos Santos, M. H. Terra, and D. F. Wolf, "Tube-based guaranteed cost model predictive control applied to autonomous driving up to the limits of handling," 2020, *arXiv:2012.05334*.
[39] C. M. Massera, M. H. Terra, and D. F. Wolf, "Guaranteed cost approach for robust model predictive control of uncertain linear systems," in *Proc. Amer. Control Conf. (ACC)*, Seattle, WA, USA, May 2017, pp. 4135–4140.
[40] J. Guo, J. Wang, P. Hu, and L. Li, "Robust guaranteed-cost path-following control for autonomous vehicles on unstructured roads," *Proc. Inst. Mech. Eng., D, J. Automobile Eng.*, vol. 232, no. 7, pp. 896–908, Jun. 2018.

KANGLE HU received the B.S. degree in mechanical engineering from Jilin University, Changchun, China, in 2016, where he is currently pursuing the Ph.D. degree with the School of Mechanical and Aerospace Engineering. His research interests include vehicle dynamics, vehicle motion control, and the hydraulic system design.

KAI CHENG received the Ph.D. degree in mechanical design from the Jilin University of Technology, Changchun, China, in 1999. He is currently a Professor at the School of Mechanical and Aerospace Engineering, Jilin University, Changchun. His research interests include performance analysis, lightweight design, reliability of engineering machinery, and special constructing vehicle.